Temporally restricted activities of *En1* regulatory elements underlie distinct limb malformations

Alessa R. Ringel[1,2,*], Andreas Magg[1,2,3,*], Natalia Benetti[1], Robert Schöpflin[1,4], Mira Kühnlein[1], Asita Carola Stiege[1], Ute Fischer[1], Lars Wittler[5], Stephan Lorenz[6], Stefan Mundlos[1,2,3,#] & Lila Allou[1,7,8,9,#]

[1]RG Development and Disease, Max-Planck Institute for Molecular Genetics, Berlin, Germany

[2]Institute for Medical and Human Genetics, Charité-Universitätsmedizin Berlin, Berlin, Germany

[3]Berlin-Brandenburg Center for Regenerative Therapies, Charité-Universitätsmedizin Berlin, Berlin, Germany

[4]Department of Computational Molecular Biology, Max-Planck Institute for Molecular Genetics, Berlin, Germany

[5]Department of Developmental Genetics, Max-Planck Institute for Molecular Genetics, Berlin, Germany

[6]Sequencing Core Facility, Max-Planck Institute for Molecular Genetics, Berlin, Germany

[7]Developmental Neurosciences Department, UCL Great Ormond Street Institute of Child Health, Faculty of Population Health Sciences, University College London, London, UK

[8]Medical Research Council (MRC) Laboratory of Medical Sciences (LMS), London, UK

[9]Institute of Clinical Sciences, Faculty of Medicine, Imperial College London, London, UK

[*]Contributed equally

[#]Correspondence: mundlos@molgen.mpg.de; l.allou@lms.mrc.ac.uk

Abstract

The precise spatiotemporal expression of developmental genes is required for proper embryonic development. EN1 plays a key role in dorsal-ventral patterning in mouse limb development from embryonic day (E) 9.5 to E11.5. Previously, we identified the lncRNA locus *Maenli* which drives *En1* expression at E9.5, specifically in the limb. Here we addressed how *En1* expression is maintained at later developmental stages when *Maenli* transcriptional activity is absent. With a series of *in vivo* CRISPR editing, we demonstrate that at later stages E10.5 and E11.5, *En1* expression is driven by two intergenic enhancer elements, LSEE1 and LSEE2. Upon simultaneous loss of these two enhancers, mice only exhibit a subset of the *En1* mutant and *Maenli*$^{-/-}$ limb malformations. We show that the timing of *En1* misexpression during limb development causes distinct phenotypes. These findings demonstrate that the temporally restricted activities of *cis*-regulatory elements, including lncRNA loci and enhancers, may underlie subtle differences in complex disease phenotypes.

Introduction

Healthy embryonic development relies on the precise expression of genes in space and time. The spatiotemporal regulation of developmental genes is coordinated through the action of *cis*-regulatory elements (CREs) including enhancers[1] and long non-coding RNA (lncRNA) loci[2, 3]. Enhancers are short non-coding DNA sequences which increase the rate of transcription from promoters and are located at varying distances from their target genes[1, 4]. The interaction between enhancers and their target promoters is enabled by folding of the chromatin[5, 6]. Upon enhancer activation, transcription factors bind to the chromatin, facilitate the removal of nucleosomes, and recruit co-activators[4]. Active enhancers are associated with the specific histone modifications H3K27ac and H3K4me1[4]. Some lncRNA loci, encoding transcripts longer than 500 bp, act as CREs and have been reported to regulate tissue-specific developmental gene expression[2, 3].

Developmental genes are often regulated by a complex interplay of multiple enhancers that can cooperate in additive, synergistic, or redundant manners[7, 8]. Here, we deployed an *in vivo* CRISPR/Cas genome-engineering approach to dissect the regulatory architecture of the *engrailed-1* (*En1*) gene during limb development. *En1* encodes the homeobox transcription factor EN1 which can act as both a transcriptional activator and a repressor[9]. It is involved in regionalization during early embryogenesis. As such, its precise expression in space and time ensures the proper production of several tissues such as bone, muscle, cartilage, and skin[9]. *En1* is first expressed at embryonic day (E) 8 in the mouse, in the midbrain/hindbrain junction. At E9.5, it accumulates in several other tissues, including the mesenchyme adjacent to the midbrain/hindbrain junction, the developing pituitary gland, the somites, and the limb buds. In the limbs it is specifically expressed in the ventral ectoderm and apical ectodermal ridge[9]. It is also expressed in other structures from E10.5[9].

Homozygous *En1* knockout mice die shortly after birth and display multiple developmental abnormalities, including brain and skeletal (sternum, rib and limb) defects[9, 10]. The limb phenotype manifests as polydactyly and syndactyly[9, 10]. Deleting only the homeobox-coding sequence of *En1* allows rare survival of mice which display a double dorsal limb phenotype; consisting of the dorsalization of ventral structures (ventral or circumferential claws, ventral hairs, loss of pads, ventral digits, hyperpigmentation), as well as poly- and syndactyly[11, 12]. These early reports described the defects as embryonic (syn- and polydactyly) and postnatal (double dorsal) limb

phenotypes. However, as the embryonic phenotype is also present postnatally, in this study we refer to the poly-/syndactyly and double dorsal limb defects as *early* and *late* phenotypes respectively.

Although the phenotypic consequences of *En1* loss in the embryonic limb have been well characterized[13], less is known about the regulatory elements controlling *En1* expression in this tissue. *En1* is positioned in a ~ 650 kilobase (kb) topologically associated domain (TAD). TADs are genomic regions that interact with themselves more frequently than with the rest of the genome[14, 15]. In the *En1* TAD, we previously identified the lncRNA locus *Maenli* (Master activator of *engrailed-1* in the limb) which drives *En1* expression in the mouse limb bud at E9.5[13]. After initiating *En1* expression, *Maenli* transcriptional activity significantly decreases at E10.5 and E11.5 but *En1* expression is maintained[13]. This suggests that additional regulatory elements may be required to maintain *En1* expression after E9.5.

Here, we employed *in vivo* CRISPR/Cas9 genome editing to elucidate the regulatory elements responsible for maintaining *En1* expression. We have identified two enhancer elements which cooperate to drive *En1* expression in the E10.5 and E11.5 limb bud that we term Late Stage *Engrailed-1*-associated limb-specific Enhancers 1 and 2 (LSEE1 and LSEE2). Strikingly, simultaneous homozygous deletion of *LSEE1&2* causes morphological limb defects resembling only the late-stage *En1* mutant limb abnormalities[10]. In contrast, *Maenli*$^{-/-}$ mice recapitulate both the early- and late-stage morphological limb defects, supporting a distinct spatiotemporal contribution of the CREs in controlling *En1* expression. Our findings show that LSEE1&2 play a crucial role in sustaining *En1* expression during limb development. This study highlights how CREs acting in a time-specific manner can contribute to genetic disorders with subtle phenotypic variations.

Results

Deletion of the genomic region between *Maenli* and *En1* causes a loss of *En1* expression in E10.5 and E11.5 limb buds

To investigate whether additional regulatory elements drive *En1* expression in E10.5 limb buds, we performed a genetic dissection of the *En1* regulatory landscape using *in vivo* CRISPR/Cas9 genome editing. We generated two large deletions (*Del1* and *Del2*) within the *En1* regulatory

landscape, and a deletion of the *Maenli* locus itself (*Del3*) **(Fig. 1a)**. *Del1* includes the genomic region between *En1* and *Maenli* while *Del2* includes the genomic region between *Maenli* and the telomeric boundary of the *En1* TAD **(Fig. 1a)**.

In this study, qPCR analyses have been performed using *Rsp9* as a housekeeping gene to normalize the expression levels of our target genes. We also used *Gapdh* as an endogenous control for all our qPCR measurements and observed no changes in *Gapdh* levels. These analyses showed that *Del1* and *Del2* did not affect *Maenli* expression in the E9.5 limb bud **(Extended Data Fig. 1a, b)**. However, although *Del1* did not significantly affect *En1* expression in the E9.5 limb bud, expression was significantly decreased at E10.5 and E11.5 **(Fig. 1 b and Extended Data Fig. 1b, c)**. *Del2* caused a significant increase in *En1* expression at all three developmental stages **(Fig. 1 b and Extended Data Fig. 1b, c)**.

Interestingly, *Del1* mice showed strong limb malformations resembling those previously described for *En1* mutant[10, 11] and *Maenli*$^{-/-}$[13] mice. Notably, these mice exhibited the late-stage (~ 4 weeks postnatal) morphological limb defects consisting of dorsalization of ventral structures, including ventral or circumferential claws, ventral hairs, and loss of pads. However, they did not exhibit the early-stage (< 0 days postnatal) morphological limb abnormalities, including syndactyly, polydactyly, and ventral digits **(Fig. 1c, d and Extended Data Fig. 1d, e)**. These data suggest that *Del1* harbours regulatory elements driving *En1* expression in the E10.5 and E11.5 limb bud, with their loss only causing the late-stage *En1* mutant limb phenotype.

A second locus-specific lncRNA, *Lmer*, is dispensable for *En1* expression in the limb

To identify potential regulatory elements within *Del1* driving *En1* expression at E10.5 and E11.5, we first performed capture Hi-C (cHi-C) in E10.5 limb buds **(Fig. 2a)**. We examined chromatin interactions between *Del1* and *En1* using the *En1* promoter as viewpoint by deriving a virtual 4C profile from the cHi-C data. However, despite strong interactions between the *En1* promoter with the other end of the *En1* TAD we found no prominent specific interaction with a particular region in *Del1* **(Fig. 2a)**.

We then searched for putative enhancers and transcripts in *Del1* by analysing our own and previously published[16] assay for transposase-accessible chromatin, followed by sequencing (ATAC-seq) data in E10.5 and E11.5 limb buds. We found that *Del1* contains 45 putative enhancers

in the limbs as defined by ATAC-seq peaks **(Fig. 2b)**. We also performed poly(A)$^+$ RNA sequencing (RNA-seq) in wildtype E10.5 and E11.5 limb buds, somites, and the midbrain/hindbrain junction. These analyses revealed the presence of a transcript in the limb buds and the midbrain/hindbrain junction within *Del1* that was not detected in the somites **(Fig. 2c and Extended Data Fig. 2a)**. PhyloCSF analysis showed that this transcript lacks protein-coding potential, suggesting that it is a lncRNA **(Extended Data Fig. 2b)**. This is supported by the low conservation of its nucleotide sequence, which displays 28% similarity between mice and humans and low conservation across other species **(Extended Data Fig. 2b)**. We named this lncRNA locus *Lmer* (Limb midbrain/hindbrain junction expressed RNA) **(Fig. 2c)**.

The mouse *Lmer* locus encompasses 11 exons spanning approximately 76 kb and is located around 6 kb downstream of the 3'-end of *En1* **(Fig. 2d)**. Its transcriptional start site (TSS) overlaps with H3K4me3 marks in E10.5 and E11.5 limb buds and the midbrain/hindbrain junction **(Fig. 2c)**. To test whether the *Lmer* locus is required for *En1* expression and limb development *in vivo*, we generated a deletion encompassing the entire *Lmer* locus (*Del4*) **(Fig. 2d)**. This deletion did not significantly affect *En1* expression in E10.5 limb buds **(Fig. 2e)**. Thus, the mouse *Lmer* locus is dispensable for the correct timing and location of *En1* expression during limb development.

Defining the minimal critical region harbouring *En1* regulatory elements in E10.5 and E11.5 limb buds

We next hypothesized that the genomic region between *Lmer* and *Maenli* (~ 157 kb) contains regulatory elements controlling *En1* expression in E10.5 and E11.5 limb buds. This genomic region contains 28 putative enhancers in the limbs as defined by ATAC-seq peaks **(Fig. 2b)**. To determine the position of potential *En1* regulatory elements within this large genomic region, we analysed the phenotypic differences between three mutants (*Del1* and *Del3* generated in this study, and *Del27* generated in our previous study[13]) **(Extended Data Fig. 3a)**. Interestingly, while all of these mutants exhibited limb abnormalities resembling those of *En1* mutant mice[10, 11], they showed small but noticeable phenotypic differences. In *Del27* mice, limb defects were fully penetrant in the early (i.e., syndactyly, polydactyly) and late (i.e., ectopic ventral nails) developmental stages. In *Del3* mutants, however, the early- and late-stage limb abnormalities were not fully penetrant. Finally, in *Del1* mice, the early-stage limb defects were not observed with the late-stage limb abnormalities

fully penetrant **(Extended Data Fig. 3a)**. These observations suggest temporal differences in *En1* expression in the developing limb buds of the three mutants.

To test this, we quantified *En1* expression in E9.5, E10.5, and E11.5 *Del3* limb buds **(Extended Data Fig. 3b)** and also performed RNA-seq in E9.5, E10.5, and E11.5 *Del3* and *Del27* limb buds **(Extended Data Fig. 3c)**. Quantification of *En1* expression in *Del3* embryonic limbs showed an almost complete loss of *En1* expression at E9.5 with a reduction in expression levels at E10.5 and E11.5 (~ 35% and ~ 62% of wildtype respectively) **(Extended Data Fig. 3b, c)**. Moreover, RNA-seq in *Del27* limb embryos showed a complete loss of *En1* expression at all three developmental stages **(Extended Data Fig. 3c)**. These data demonstrate that *Del27* contains the complete regulatory information required to control *En1* expression during limb development. In contrast, deletion of *Maenli* alone (*Del3*) leads to only a partial loss of *En1* expression in E10.5 and E11.5 limb buds. This confirms that additional regulatory elements are required to control *En1* expression at these later stages. In combination with the results from the *Del1* mutants **(Fig. 1 b and Extended Data Fig. 1b, c)**, these findings suggest that putative regulatory elements located within the overlapping genomic region between *Del1* and *Del27* control *En1* expression in the limb buds after E9.5.

LSEE1 and LSEE2 are required for the maintenance of *En1* expression and proper limb development

The overlapping 6 kb genomic region between *Del1* and *Del27* contains two putative enhancer elements as defined by vertebrate conservation measured using Genomic Evolutionary Rate Profiling (GERP) and ATAC-seq **(Fig. 3a)**. We generated a ~ 2 kb deletion of one of the putative enhancers (*Del5*), which caused a significant decrease in *En1* expression by ~ 23% in E10.5 mutant limb buds **(Fig. 3a, b)**. This reduction in *En1* expression was not as severe as in E10.5 limb buds of the *Del1* mutants encompassing the two putative enhancers **(Fig. 1b and Extended Data Fig. 1c)**. Therefore, we next generated a ~ 4 kb deletion covering both putative enhancers (*Del6*) **(Fig. 3a)**. This significantly decreased *En1* expression in E10.5 and E11.5 limb buds (~ 77% and ~ 91% reduction respectively) **(Fig. 3c, d)**. *Del6* mutants display the same reduction in *En1* expression in E10.5 and E11.5 limb buds as *Del1* mutants, as well as the same late-stage limb malformations **(Fig. 1b, 3e and Extended Data Fig. 1c)**. Indeed, these mice exhibited limb defects consisting of dorsalization of ventral structures, including ventral or circumferential claws, ventral hairs, and

loss of pads. However, we did not observe syndactyly, polydactyly, and ventral digits resembling the early-stage morphological limb abnormalities **(Fig. 3e)**. These data indicate that the deleted region (*Del6)* contains enhancers which cooperate to drive *En1* expression in the E10.5 and E11.5 limb buds. We named these two enhancer elements LSEE1 and LSEE2 (Late Stage *Engrailed-1*-associated limb-specific Enhancer) respectively **(Fig. 3a)**. Given that LSEE1&2 are positioned ~ 2.5 kb upstream of *Maenli*, we next examined whether the initial transcriptional activity of *Maenli* at E9.5 is needed for the downstream activity of LSEE1&2. We generated a ~ 235 kb inversion moving the enhancers away from the 3' end of *Maenli* and close (~ 4 kb) to the 3' end of *En1* (*Inv*) **(Extended Data Fig. 4a)**. This inversion did not significantly affect *En1* expression in E11.5 limb buds **(Extended Data Fig. 4b)**, suggesting that LSEE1&2 enhancer activity may not depend on the initial transcriptional elongation through the *Maenli* locus.

Discussion

We previously characterized the lncRNA locus *Maenli* as the master activator of *En1* expression in the mouse limb bud at E9.5. Here, we show that *En1* expression is maintained at later developmental stages by two enhancers, LSEE1 and LSEE2. Overall, we show that *En1* expression throughout limb development is regulated by the coordinated action of both a lncRNA locus and enhancers over time. To our knowledge, this is the first instance of time-specific gene regulation within the same tissue being linked to distinct congenital malformations.

Deleting the genomic region between *Maenli* and the telomeric end of the *En1* TAD (*Del2*) significantly increased *En1* expression during limb development **(Fig. 1b and Extended Data Fig. 1c)**. This deletion shifts the telomeric TAD boundary closer to CREs of *En1*, possibly increasing their contact frequency with the *En1* promoter, leading to its upregulation. By contrast, removal of the region between *En1* and *Maenli* (*Del1*) significantly reduced *En1* expression in the E10.5 and E11.5 limb bud **(Fig. 1b and Extended Data Fig. 1c)**. In this region we found another lncRNA locus which we thought may regulate *En1* at later stages. However, we found this lncRNA locus, *Lmer*, to be dispensable for limb development (*Del4*) **(Fig. 2e)**. Instead, *Lmer* is highly expressed in the midbrain/hindbrain junction, where *En1* is also expressed and is essential for its development[9] **(Fig. 2c)**. How *En1* expression is controlled in this linear structure between the two brain regions is unknown. Hence, it is tempting to speculate that *Lmer* controls *En1* expression in the midbrain/hindbrain junction.

With further deletions we identified a ~ 6 kb genomic region containing the LSEE1&2 enhancers required for maintaining *En1* expression after E9.5 **(Fig. 3a, b, c, d and Extended Data Fig. 3a, b, c)**. Homozygous deletion of LSEE1&2 resulted in up to 91% loss of *En1* expression in E11.5 limb buds **(Fig. 3d)**. Although we do not know whether LSEE1&2 cooperate redundantly, additively, or synergistically, it seems that their function is reliant on *Maenli* transcriptional activity. Deletion of *Maenli* and LSEE1&2 together (*Del27*) fully ablates *En1* expression in the limb **(Extended Data Fig. 3c)**. However, the presence of only LSEE1&2 in *Del3* (homozygous deletion of *Maenli*) limb mutants causes a ~92% reduction in *En1* expression at E9.5, but recovers to ~62% by E11.5 **(Extended Data Fig. 3b, c)**. This suggests either that *En1* at later stages is driven by a combination of the enhancers and residual *Maenli* activity[13] or that *Maenli* activity itself is required for the full activity of the enhancers.

A complex regulatory architecture with inter-dependencies on multiple *cis* regulatory elements *in vivo* has been reported only for few genes including *Sox9*[17]. *Sox9* plays a crucial role in sex determination where its transcription in the gonads relies on an enhancer cascade involving the activity of an early-enhancer that is required for later enhancer activation[17]. Here we also see a temporal interplay of CRE activity at the *En1* locus where the activity of *Maenli* may be required for later enhancer activity. Based on the following two lines of reasoning, we hypothesize a transcription-based mechanism underlies LSEE1&2 activation. Firstly, we previously showed that insertion of a polyadenylation termination sequence shortly after the *Maenli* transcription start site ablated *En1* expression and H3K4me3 deposition across the *Del1* region[13]. However, inversion of this polyadenylation termination sequence did not affect *En1* wildtype levels. Although these experiments cannot distinguish between the act of *Maenli* transcription and the function of the transcript itself, they suggest that a transcriptional mechanism underlies *En1* activation and the establishment of a permissive chromatin state. Secondly, in this study we show that inverting the *Del1* region to bring LSEE1&2 ~300kb away from *Maenli* had no effect on *En1* expression **(Extended Data Fig. 4)**, indicating that *Maenli* transcription *per se* is not needed for LSEE1&2 activation. However, since this inversion placed LSEE1&2 ~4kb downstream of *En1* **(Extended Data Fig. 4)**, transcriptional elongation originating from *En1* may be sufficient for their activation. Thus, we cannot rule out a transcription-based mechanism of enhancer activation.

Another hypothesis is that *Maenli´*s promoter could be a *cis*-acting transcriptional stabilizer of *En1*. In this scenario, close physical proximity of the *Maenli* promotor with the *En1* promoter would

also bring LSEE1&2 close to *En1*, therefore allowing them to sustain *En1* expression. Indeed, *Maenli* and *En1* are in close proximity with one another in the E9.5 limb bud[13]. This type of regulatory mechanism has been reported for the lncRNA locus *HASTER* which drives the interaction of enhancers with its adjacent target gene, *HNF1a*[18]. Alternatively, *En1* expression could be maintained during limb development through a positive feedback loop where the transcription factor EN1 binds to its own enhancers LSEE1&2. Residual *En1* expression (~8%) in the absence of *Maenli* (*Del3*) could be sufficient to facilitate a low level of enhancer activity which would explain the partial recovery of *En1* expression at later stages **(Extended Data Fig. 3b, c)**. Such a positive feedback mechanism has been reported for LMX1B where it binds to two conserved *Lmx1b*-associated CREs which in turn amplify *Lmx1b* expression during limb dorsalization[19]. A more complex reinforcing feedback loop is also possible, where EN1 activates other transcription factors involved in ventral ectoderm and apical ectodermal ridge specification. Such a mechanism has been reported for *Fgf8* and *Fgf10* during limb development[20]. FGF10 signaling triggers the expression of *Fgf8* in the ectoderm through a positive regulatory loop, possibly coordinated via gene regulatory components.

En1 mutation experiments from the 90s revealed distinct early (syndactyly, polydactyly) and late (double-dorsal) limb phenotypes in mice[12, 21]. Our previously reported mutant mice that lack *Maenli* and the here identified enhancers LSEE1&2 (*Del27*) displayed a fully penetrant phenotype consisting of both early and late-stage morphological phenotypes[13]. However, mice with only the *Maenli* deletion (*Del3*) exhibit the same limb abnormalities but without being fully penetrant **(Fig. 1c, d and Extended Data Fig. 1d, e)**, suggesting that LSEE1&2 partially rescue *En1* expression in the absence of *Maenli*. Interestingly, mice lacking LSEE1&2 only display the late-stage morphological phenotype (**Fig. 1c, d, 3e and Extended Data Fig. 1d, e)**, suggesting that *En1*´s role at E9.5 is not affected, when establishment of proper digit number and separation occurs. Such a temporally restricted function of *En1* has also been suggested by homozygous replacement of *En1* with *En2*, which causes only the late-stage morphological phenotype[12, 21]. This suggests that the biochemical function of EN2 is able to compensate for that of EN1 for patterning proper digit number and separation, but not dorsal-ventral patterning. Here we show that these distinct temporal roles of *En1* are controlled by the coordinated function of *Maenli* and LSEE1&2 **(Fig. 4)**. However, to uncover the precise molecular mechanism(s) of *Maenli* and LSEE1&2 enhancer function and interplay further studies are necessary. One major limiting factor to these studies is the restriction

of *En1* expression to a small number of cells in the limb bud (ventral ectoderm and apical ectodermal ridge) and the low level of *Maenli* expression.

Overall, our findings have important implications for congenital limb malformations which are common[22] and frequently isolated. The diagnostic yield in these cases remains low due to, at least in part, a focus on studying coding sequences. Our previous findings and others have shown that tissue-specific CREs are potential candidates to explain these isolated limb malformations[13, 19, 23, 24, 25, 26]. The findings of this study support the notion that time-specific CREs, including lncRNA loci and enhancers, are potential candidates for explaining isolated limb malformations with subtle phenotypic differences. Here we extend previous reports[18, 27, 28, 29] by describing the coordinated action of a lncRNA locus and enhancers to control temporal gene expression. To our knowledge, this is the first study linking this temporal gene regulation to distinct phenotypes.

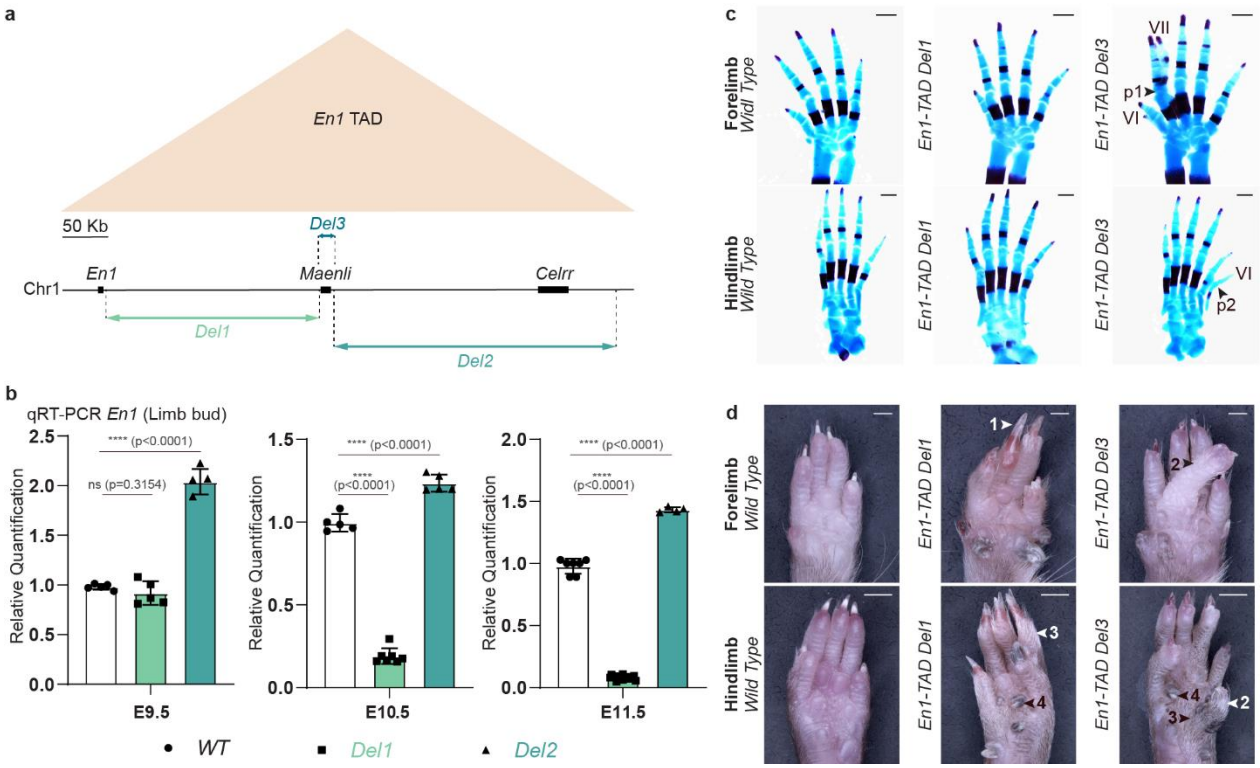

Figure 1. *Del1* significantly decreases *En1* expression in the limb and causes a double dorsal limb phenotype in mice. a, Schematic representation of the *En1* TAD (beige triangle) and the CRISPR-Cas9 genetic dissection of the *En1* regulatory landscape (*Del1*, *Del2*, and *Del3*). **b,** Normalized qRT-PCRs of *En1* in E9.5, E10.5, and E11.5 limb embryos show a significant loss of *En1* expression at E10.5 and E11.5 upon deletion of the genomic region between *En1* and *Maenli* (*Del1*). By contrast, this deletion did not significantly affect *En1* expression at E9.5. Deletion of the genomic region between *Maenli* and the telomeric end of the *En1* TAD (*Del2*) resulted in a significant increase of *En1* expression at E9.5, E10.5, and E11.5, respectively. Data were normalized to wild-type expression; one-tailed t-test; data are mean±SD; n ≥ 3 biologically independent wild-type and mutant limb pairs. ns, non-significant; *, ($p < 0.01$); p, p-value; WT, wild-type. **c,** Alcian blue (cartilage) and alizarin red (bone) stained limbs prepared from wild-type, *Del1*, and *Del3* E18.5 embryos. The *Del1* mutant is indistinguishable from the wild-type. The *Del3* mutant exhibits the presence of a polydactyly (digit VI) and an ectopic ventral digit (VII) fused at the level of phalange 1 in the forelimb, and an ectopic ventral digit (VI) fused at the level of phalange 2 in the hindlimb. p, phalange. Scale bars, 500 µm; n ≥ 3 biologically independent wild-type and mutant limb pairs. **d,** Ventral views of wild-type, *Del1*, and *Del3* adult (8-weeks) fore- and hindpaws illustrating the presence of ectopic ventral nails that manifest as circumferential nails (1), ectopic ventral digits (2), and ectopic ventral hairs (3). The pigmented metatarsal pads (4) are elongated and hardened, resembling nails. Scale bars, 1,000 µm for forelimbs and 2,000 µm for hindlimbs, respectively; n ≥ 3 biologically independent wild-type and mutant limb pairs.

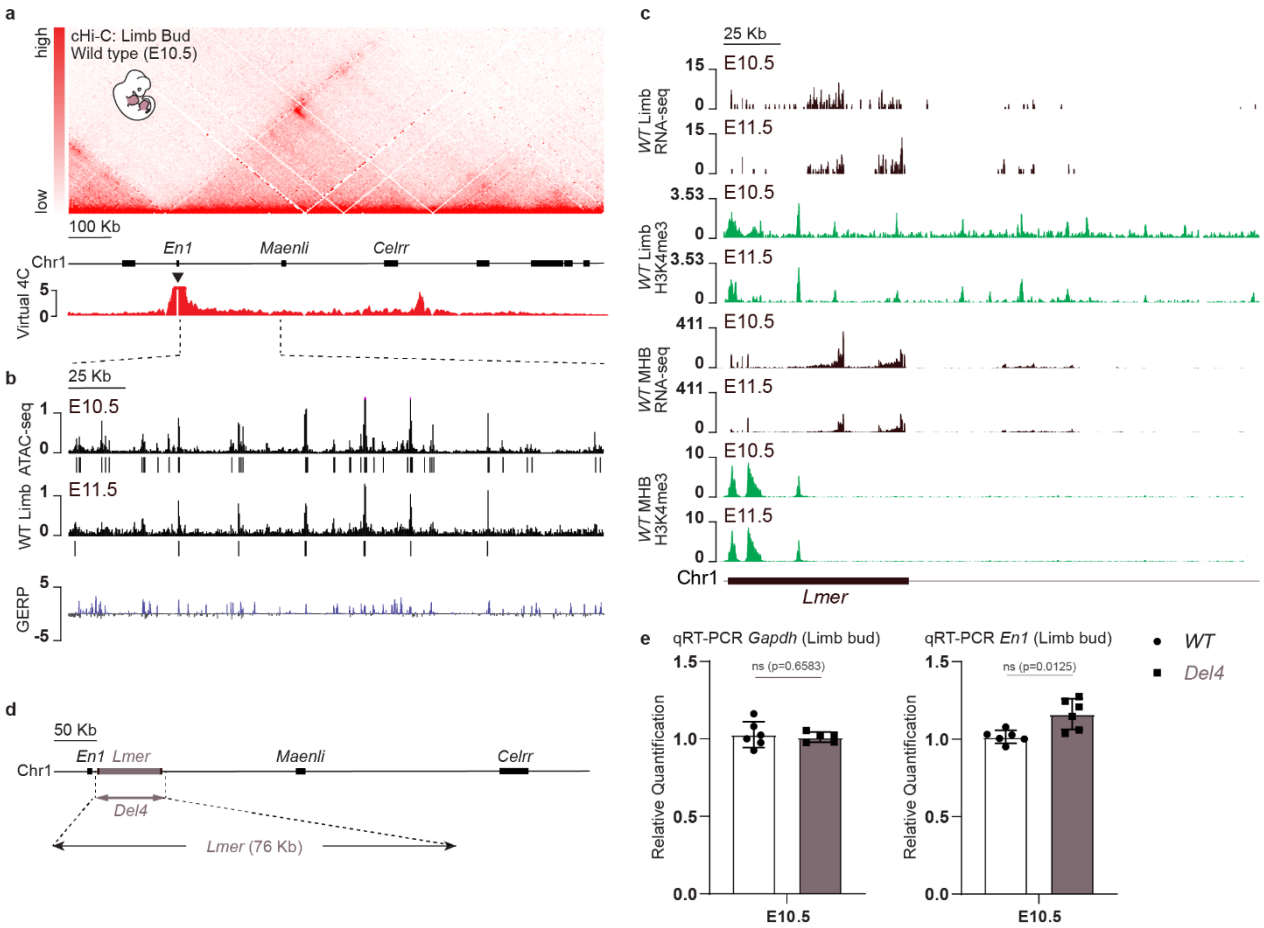

Figure 2. *Lmer* is dispensable for *En1* expression regulation during limb development. a, cHi-C map of the mouse limb buds at E10.5 shows a large TAD encompassing the *En1* gene and the *Maenli* and *Celrr* lncRNA loci. Virtual 4C profile using the *En1* promoter as viewpoint (black triangle) shows no prominent interaction between *En1* and the genomic region upstream of *Maenli*. **b,** ATAC reads from wild type (WT) E10.5 and E11.5 mouse limb buds are shown. Peak calling identifying genomic regions which are enriched in aligned ATAC reads (to a statistically significant extent) compared to background levels is also shown. **c,** Poly(A)$^+$ RNA-seq and H3K4me3 ChIP-seq profiles of E10.5 and E11.5 mouse limb buds and midbrain-hindbrain junction show the presence of the lncRNA locus *Lmer*. **d,** Schematic representation of the CRISPR-Cas9 genetic deletion involving the lncRNA locus *Lmer* (*Del4*). **e,** Normalized qRT-PCRs of *Gapdh* and *En1* in E10.5 mouse limb embryos show no significant changes in *Gapdh* and *En1* expression upon deleting the lncRNA locus *Lmer* (*Del4*). Data were normalized to wild-type expression; one-tailed t-test; data are mean±SD; n ≥ 3 biologically independent wild-type and mutant limb pairs. ns, non-significant; *, ($p < 0.01$); p, p-value; WT, wild-type.

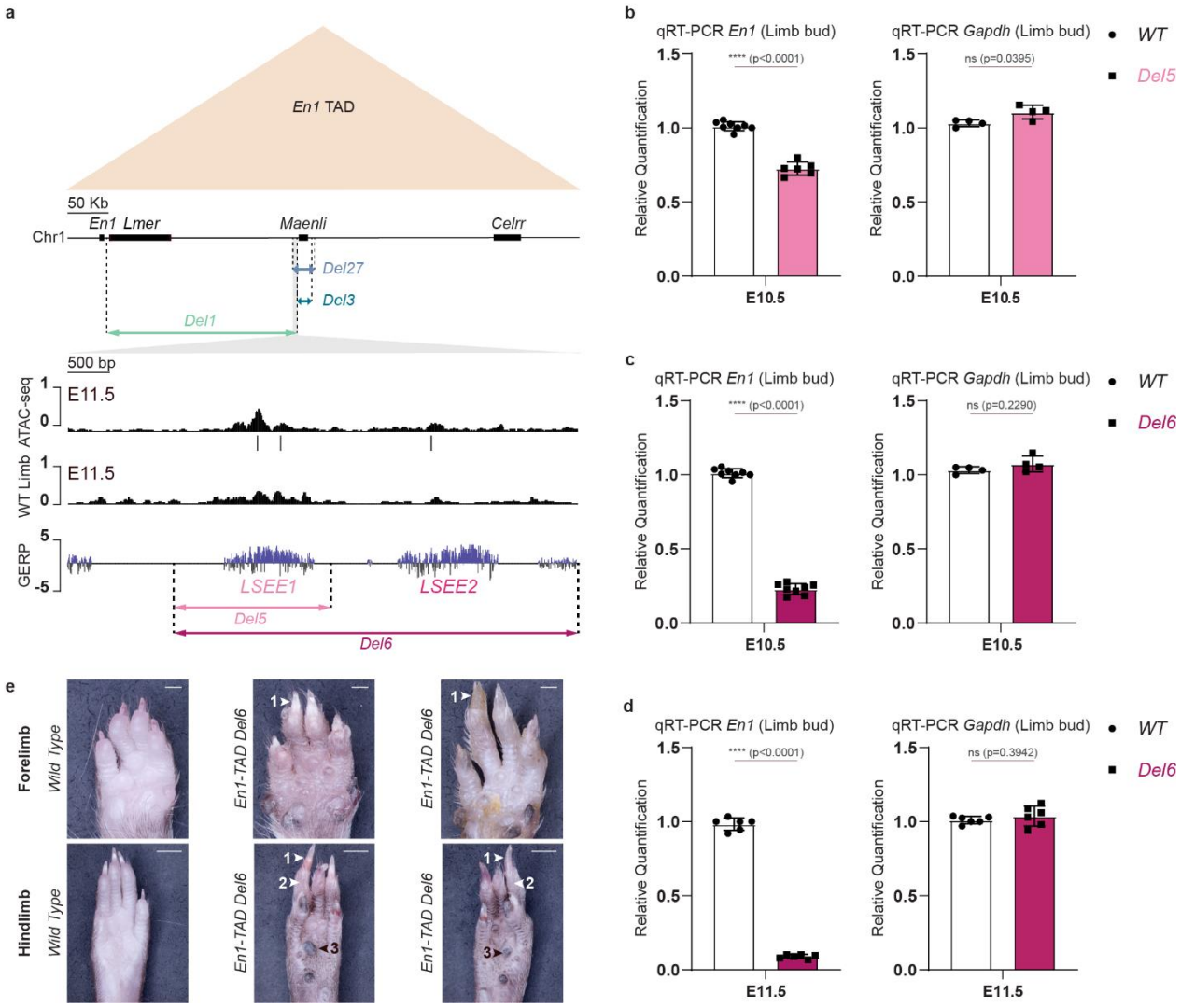

Figure 3. LSEE1 and LSEE2 enhancers cooperate to drive *En1* expression in E10.5 and E11.5 mouse limb buds. **a,** Schematic representation of the *En1*-TAD (beige triangle) and the CRISPR-Cas9 genetic deletions (*Del1*, *Del3*, and *Del27*) affecting *En1* limb expression and causing abnormal limb bud dorsoventral patterning in mice. The overlapping genomic region between *Del1* and *Del27* is highlighted in grey, and a zoom-in of the region is shown. ATAC reads from wild-type E10.5 and E11.5 mouse limb buds indicate the presence of putative enhancer elements within the overlapping genomic region. Vertebrate conservation is measured using the Genomic Evolutionary Rate Profiling (GERP) method. It indicates the presence of two highly conserved non-coding DNA elements within the overlapping genomic region. Finally, a schematic representation of the CRISPR-Cas9 genetic dissection of the overlapping genomic region (*Del5* and *Del6*) is shown. **b,** Normalized qRT-PCRs of *En1* and *Gapdh* in E10.5 mouse limb embryos show no significant changes in *Gapdh* expression, but a significant loss of *En1* expression upon deleting the single enhancer LSEE1 (*Del5*). Data were normalized to wild-type expression; one-tailed t-test; data are mean±SD; $n \geq 3$ biologically independent wild-type and mutant limb pairs. ns, non-significant; *, ($p < 0.01$); p, p-value; WT, wild-type. **c, d,** Normalized qRT-PCRs of *En1* and *Gapdh* in E10.5 and E11.5 mouse limb buds isolated from *Del6* embryos show no significant changes in *Gapdh* expression, but a significant loss of *En1* expression at both developmental stages with an almost complete loss at E11.5. Data were normalized to wild-type expression; one-tailed t-test; data are mean±SD; $n \geq 3$ biologically independent wild-type and mutant limb pairs. ns, non-significant; *, ($p < 0.01$); p, p-value; WT, wild-type. **e,** Ventral views of wild-type and *Del6* adult (6-weeks) fore- and hind-paws illustrating the presence of ectopic ventral nails that manifest as circumferential nails (1) and ectopic ventral hairs (2). The pigmented metatarsal

pads (3) are elongated and hardened, resembling nails. Scale bars, 1,000 µm for forelimbs and 2,000 µm for hindlimbs, respectively; $n \geq 3$ biologically independent wild-type and mutant limb pairs.

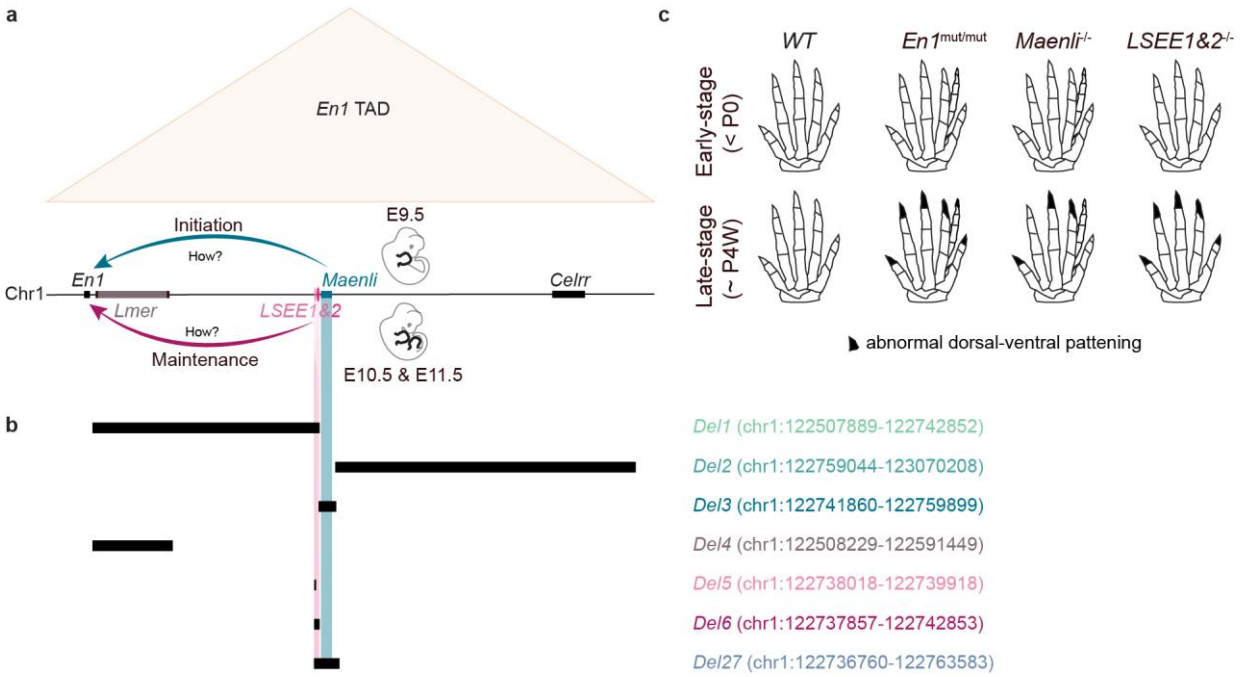

Figure 4. A model for limb-specific *En1* expression regulation. a, During limb development, *Maenli*, LSEE1, and LSEE2 fine-tune temporal *En1* expression. The lncRNA locus *Maenli* licenses *En1* expression specifically at E9.5. LSEE1&2 enhancers cooperate to drive *En1* expression, specifically at E10.5 and E11.5. The molecular mechanisms of *En1* expression control by *Maenli* and LSEE1&2 remain unknown (?). **b,** Schematic representation of the CRISPR-Cas9 genetic deletions. The extent of each deleted genomic region in mice is given as mm9 coordinates. **c,** Schematic representation of *Maenli*$^{-/-}$ and *LSEE1&2*$^{-/-}$-associated limb phenotypes. *Maenli*$^{-/-}$ and *LSEE1&2*$^{-/-}$ mice exhibit limb defects recalling those of *En1* mutant mice. However, while *Maenli*$^{-/-}$ mutants exhibit early- and late-stage morphological limb defects, *LSEE1&2*$^{-/-}$ mutants exhibit only late-stage morphological limb abnormalities. Differential phenotypic features between *En1* mutant, *Maenli*$^{-/-}$, and *LSEE1&2*$^{-/-}$ mice include the polydactyly and/or syndactyly, which is fully penetrant in *En1* mutants, not fully penetrant in *Maenli*$^{-/-}$ mice, and absent in *LSEE1&2*$^{-/-}$ mutants. On the other hand, ectopic ventral nails are fully penetrant in both *En1* mutant and *LSEE1&2*$^{-/-}$ mice and not fully penetrant in *Maenli*$^{-/-}$ mutants. P0, postnatal day 0; P4W, 4 weeks postnatally.

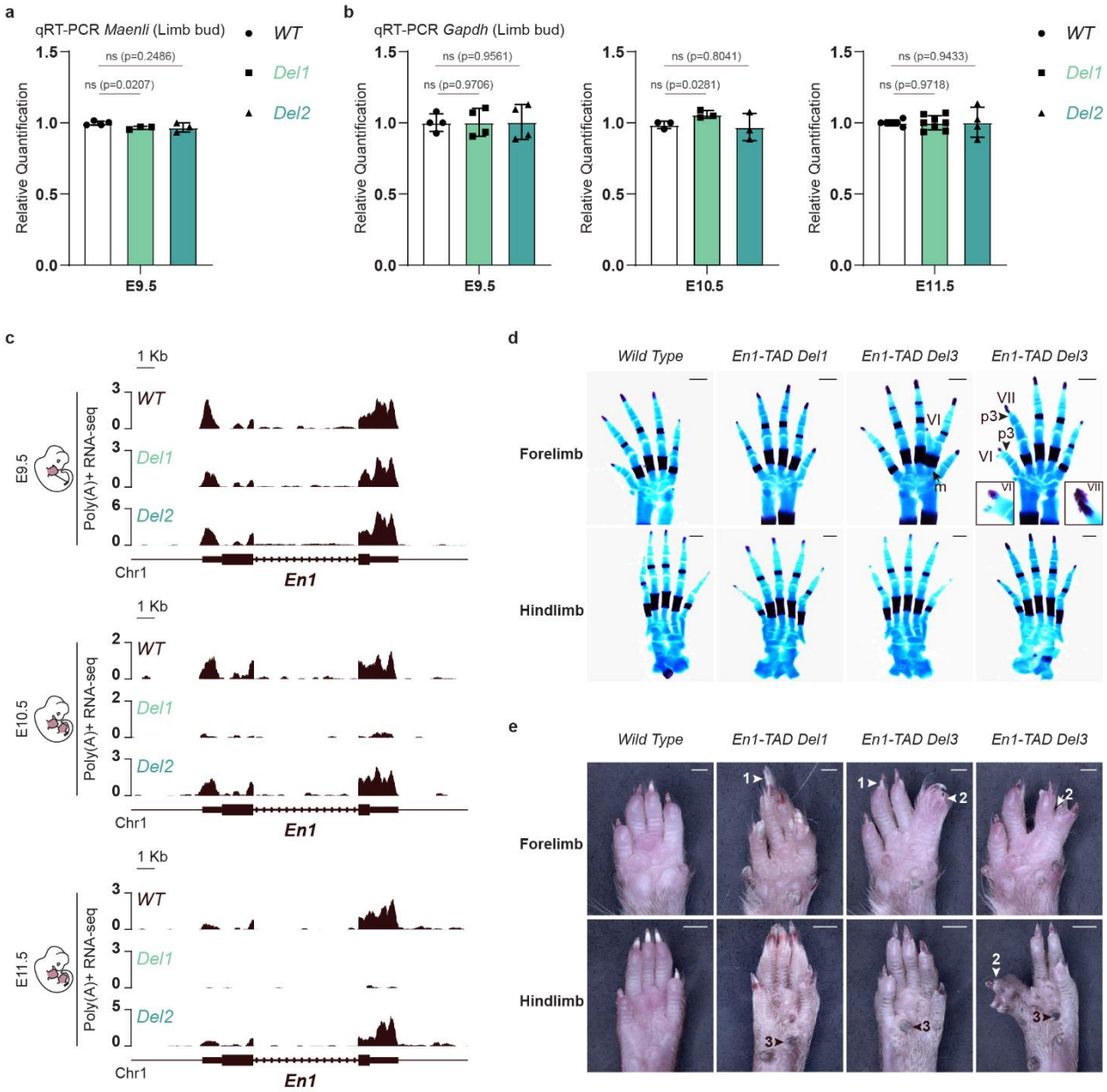

Extended Data Figure 1. *Del1* mouse model exhibits abnormal limb bud dorso-ventral patterning similar to *Maenli*$^{-/-}$ and *En1* mutant mice. a, Normalized qRT-PCRs of *Maenli* in E9.5 mouse limb embryos show that *Del1* and *Del2* did not significantly affect *Maenli* expression. Data were normalized to wild-type expression; one-tailed t-test; data are mean±SD; n ≥ 3 biologically independent wild-type and mutant limb pairs. ns, non-significant; *, ($p < 0.01$); p, p-value; WT, wild-type. **b,** Normalized qRT-PCRs of *Gapdh* in E9.5, E10.5, and E11.5 mouse limb embryos show no significant changes in *Gapdh* expression upon *Del1* and *Del2* deletions. Data were normalized to wild-type expression; one-tailed t-test; data are mean±SD; n ≥ 3 biologically independent wild-type and mutant limb pairs. ns, non-significant; *, ($p < 0.01$); p, p-value; WT, wild-type. **c,** Poly(A)$^+$ RNA-seq profiles of E9.5, E10.5, and E11.5 mouse limb buds show that *Del1* did not affect *En1* expression at E9.5 but resulted in an almost complete loss of *En1* expression at E10.5 and E11.5. By contrast, *Del2* increased *En1* expression at E9.5, E10.5, and E11.5. WT, wild-type. **d,** Alcian blue (cartilage) and alizarin red (bone) stained limbs prepared from wild-type, *Del1*, and *Del3* E18.5 embryos. The *Del1* mutant is indistinguishable from the wild-type. The *Del3* mutant exhibits the presence of ectopic ventral digits (VI and VII) fused at the level of metacarpal or phalanges 3 in the forelimb. m, metacarpal; p, phalange.

Scale bars, 500 μm; n ≥ 3 biologically independent wild-type and mutant limb pairs. **e,** Ventral views of wild-type, *Del1*, and *Del3* adult (8-weeks) fore- and hind-paws illustrating the presence of ectopic ventral nails that manifest as circumferential nails or ventral nails formed opposite to the dorsal nails (1), and syndactyly (2). The pigmented metatarsal pads (3) are elongated and hardened, resembling nails. Scale bars, 1,000 μm for forelimbs and 2,000 μm for hindlimbs, respectively; n ≥ 3 biologically independent wild-type and mutant limb pairs.

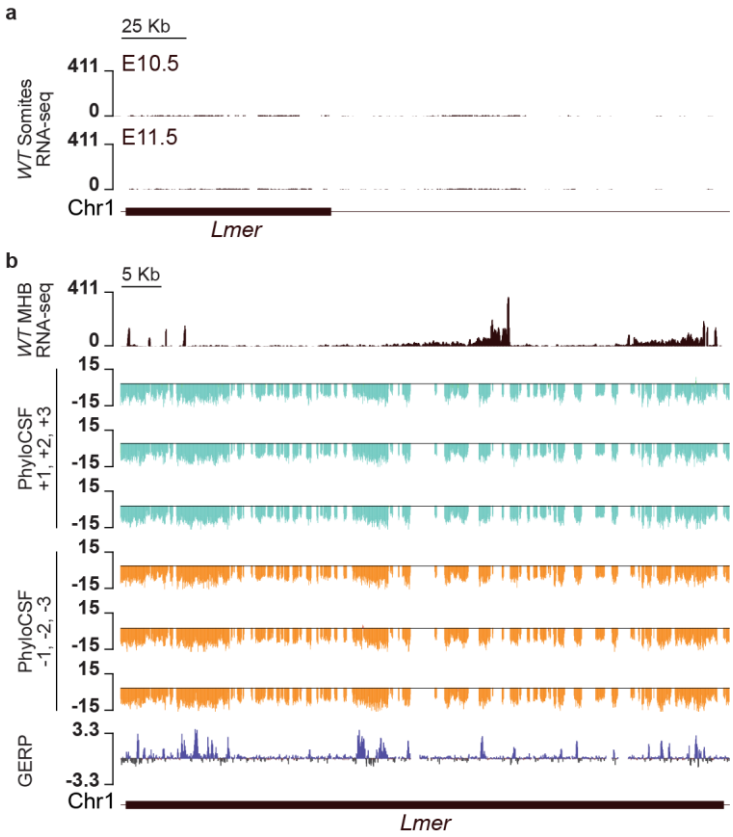

Extended Data Figure 2. *Lmer* is expressed in the limb and midbrain-hindbrain boundary but not in the somites. **a,** Poly(A)$^+$ RNA-seq profiles of E10.5 and E11.5 wild type (WT) mouse somites show no expression of *Lmer* in these embryonic structures. **b,** Poly(A)$^+$ RNA-seq profile of wild type (WT) mouse midbrain-hindbrain junction show a Zoom in of the *Lmer* transcript (exon-intron composition). PhyloCSF tracks show a lack of protein coding potential for the *Lmer* transcript. Vertebrate sequence conservation tracks measured using the Genomic Evolutionary Rate Profiling (GERP) method show that the *Lmer* nucleotide sequence (exon composition) exhibits little conservation.

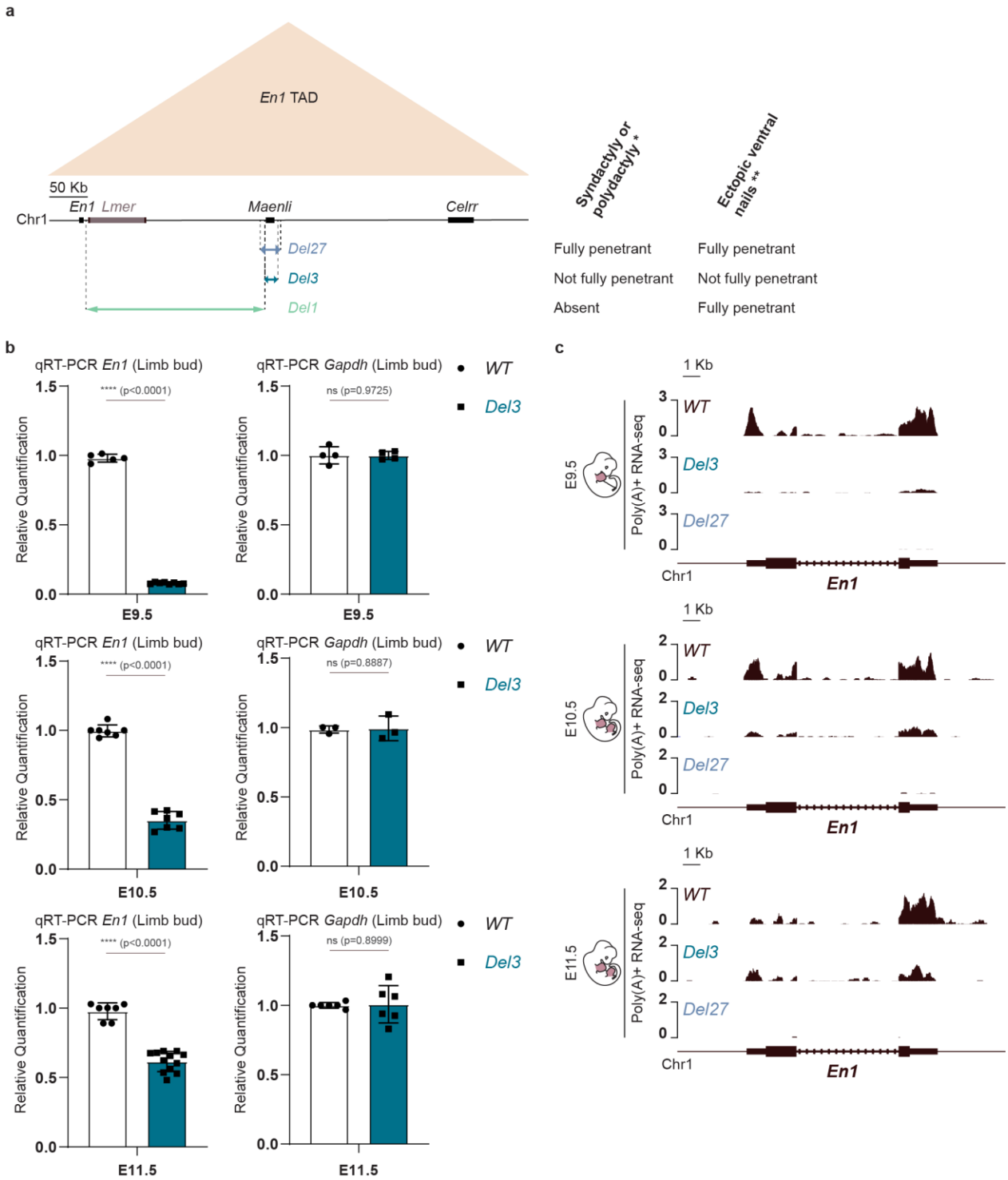

Extended Data Figure 3. The overlapping genomic region between *Del1* and *Del27* contains the putative enhancers controlling *En1* expression in E10.5 and E11.5 mouse limb buds. a, Schematic representation of the *En1* TAD (beige triangle) and the CRISPR-Cas9 genetic deletions affecting *En1* limb expression and causing abnormal limb bud dorsoventral patterning in mice. The main differential phenotypic features of the mutants at E18.5 (syndactyly or polydactyly) and 8 weeks of age (ectopic ventral nails) are shown on the right (*, penetrance is referred to the presence of polydactyly or syndactyly in all forelimbs; **, penetrance is referred to the presence of ectopic ventral nails on all digits of both forelimbs and hindlimbs). **b,** Normalized qRT-PCRs of *En1* and *Gapdh* in E9.5, E10.5, and

E11.5 mouse limb embryos show no significant changes in *Gapdh* expression upon deleting *Maenli* (*Del3*). By contrast, this deletion significantly affected *En1* expression at E9.5, E10.5, and E11.5, with an almost complete loss at E9.5. *En1* expression was partially rescued at E10.5 and E11.5. Data were normalized to wild-type expression; one-tailed t-test; data are mean±SD; $n \geq 3$ biologically independent wild-type and mutant limb pairs. ns, non-significant; *, ($p < 0.01$); p, p-value; WT, wild-type. **c,** Poly(A)$^+$ RNA-seq profiles of E9.5, E10.5, and E11.5 mouse limb buds show that *Del27* caused a complete loss of *En1* expression at all three developmental stages. *Del3* caused an almost complete loss of *En1* expression at E9.5 with a partial rescue at E10.5 and E11.5. WT, wild-type.

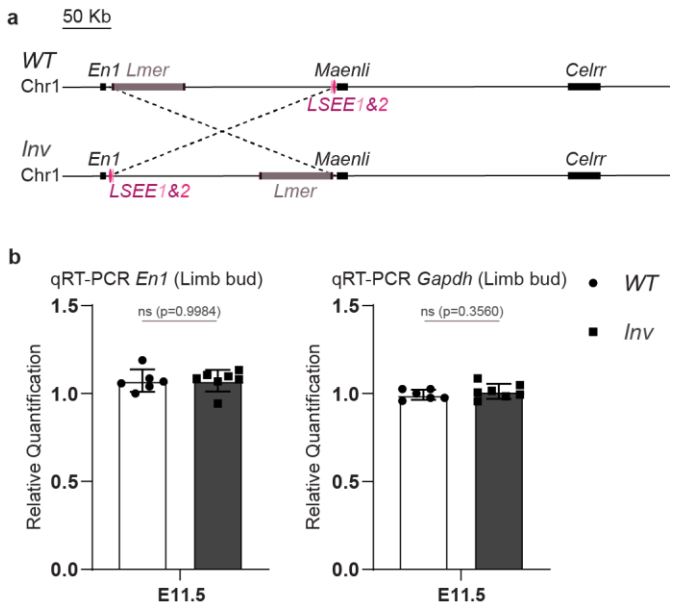

Extended Data Figure 4. LSEE1&2 enhancer activity is not dependent on transcription elongation through the *Maenli* locus. a, Schematic representation of the CRISPR-Cas9 genetic inversion repositioning the LSEE1&2 enhancers away from *Maenli* within the *En1* regulatory landscape (*Inv*). **b,** Normalized qRT-PCRs of *En1* and *Gapdh* in E11.5 mouse limb embryos show no significant changes in *En1* and *Gapdh* expression upon repositioning the LSEE1&2 enhancers away from *Maenli* (*Inv*). Data were normalized to wild-type expression; one-tailed t-test; data are mean±SD; n ≥ 3 biologically independent wild-type and mutant limb pairs. ns, non-significant; p, p-value; WT, wild-type.

1. de Laat W, Duboule D. Topology of mammalian developmental enhancers and their regulatory landscapes. *Nature* **502**, 499-506 (2013).

2. Mattick JS, *et al*. Long non-coding RNAs: definitions, functions, challenges and recommendations. *Nat Rev Mol Cell Biol* **24**, 430-447 (2023).

3. Ferrer J, Dimitrova N. Transcription regulation by long non-coding RNAs: mechanisms and disease relevance. *Nat Rev Mol Cell Biol* **25**, 396-415 (2024).

4. Serebreni L, Stark A. Insights into gene regulation: From regulatory genomic elements to DNA-protein and protein-protein interactions. *Curr Opin Cell Biol* **70**, 58-66 (2021).

5. Furlong EEM, Levine M. Developmental enhancers and chromosome topology. *Science* **361**, 1341-1345 (2018).

6. Kagey MH, *et al*. Mediator and cohesin connect gene expression and chromatin architecture. *Nature* **467**, 430-435 (2010).

7. van Arensbergen J, van Steensel B. Functional Enhancer Screening in Single Cells. *Mol Cell* **66**, 167-168 (2017).

8. Osterwalder M, *et al.* Enhancer redundancy provides phenotypic robustness in mammalian development. *Nature* **554**, 239-243 (2018).

9. Ma X, Zhao LL, Yu YC, Cheng Y. Engrailed: Pathological and physiological effects of a multifunctional developmental gene. *Genesis*, e23557 (2023).

10. Wurst W, Auerbach AB, Joyner AL. Multiple developmental defects in Engrailed-1 mutant mice: an early mid-hindbrain deletion and patterning defects in forelimbs and sternum. *Development* **120**, 2065-2075 (1994).

11. Loomis CA, Harris E, Michaud J, Wurst W, Hanks M, Joyner AL. The mouse Engrailed-1 gene and ventral limb patterning. *Nature* **382**, 360-363 (1996).

12. Hanks MC, *et al*. Drosophila engrailed can substitute for mouse Engrailed1 function in mid-hindbrain, but not limb development. *Development* **125**, 4521-4530 (1998).

13. Allou L, *et al*. Non-coding deletions identify Maenli lncRNA as a limb-specific En1 regulator. *Nature* **592**, 93-98 (2021).

14. Robson MI, Ringel AR, Mundlos S. Regulatory Landscaping: How Enhancer-Promoter Communication Is Sculpted in 3D. *Mol Cell* **74**, 1110-1122 (2019).

15. Allou L, Mundlos S. Disruption of regulatory domains and novel transcripts as disease-causing mechanisms. *Bioessays*, e2300010 (2023).

16. Paliou C, *et al.* Preformed chromatin topology assists transcriptional robustness of Shh during limb development. *Proc Natl Acad Sci U S A* **116**, 12390-12399 (2019).

17. Gonen N, *et al.* Sex reversal following deletion of a single distal enhancer of Sox9. *Science* **360**, 1469-1473 (2018).

18. Beucher A, *et al.* The HASTER lncRNA promoter is a cis-acting transcriptional stabilizer of HNF1A. *Nat Cell Biol* **24**, 1528-1540 (2022).

19. Haro E, *et al.* Identification of limb-specific Lmx1b auto-regulatory modules with Nail-patella syndrome pathogenicity. *Nat Commun* **12**, 5533 (2021).

20. Petit F, Sears KE, Ahituv N. Limb development: a paradigm of gene regulation. *Nat Rev Genet* **18**, 245-258 (2017).

21. Hanks M, Wurst W, Anson-Cartwright L, Auerbach AB, Joyner AL. Rescue of the En-1 mutant phenotype by replacement of En-1 with En-2. *Science* **269**, 679-682 (1995).

22. Giele H, Giele C, Bower C, Allison M. The incidence and epidemiology of congenital upper limb anomalies: a total population study. *J Hand Surg Am* **26**, 628-634 (2001).

23. Lettice LA, *et al.* Disruption of a long-range cis-acting regulator for Shh causes preaxial polydactyly. *Proc Natl Acad Sci U S A* **99**, 7548-7553 (2002).

24. Skuplik I, Benito-Sanz S, Rosin JM, Bobick BE, Heath KE, Cobb J. Identification of a limb enhancer that is removed by pathogenic deletions downstream of the SHOX gene. *Sci Rep* **8**, 14292 (2018).

25. Dathe K, *et al.* Duplications involving a conserved regulatory element downstream of BMP2 are associated with brachydactyly type A2. *Am J Hum Genet* **84**, 483-492 (2009).

26. Birnbaum RY, Everman DB, Murphy KK, Gurrieri F, Schwartz CE, Ahituv N. Functional characterization of tissue-specific enhancers in the DLX5/6 locus. *Hum Mol Genet* **21**, 4930-4938 (2012).

27. Isoda T, *et al.* Non-coding Transcription Instructs Chromatin Folding and Compartmentalization to Dictate Enhancer-Promoter Communication and T Cell Fate. *Cell* **171**, 103-119 e118 (2017).

28. Ritter N, *et al.* The lncRNA Locus Handsdown Regulates Cardiac Gene Programs and Is Essential for Early Mouse Development. *Dev Cell* **50**, 644-657 e648 (2019).

29. Anderson KM, Anderson DM, McAnally JR, Shelton JM, Bassel-Duby R, Olson EN. Transcription of the non-coding RNA upperhand controls Hand2 expression and heart development. *Nature* **539**, 433-436 (2016).

30. Kraft K, *et al.* Deletions, Inversions, Duplications: Engineering of Structural Variants using CRISPR/Cas in Mice. *Cell Rep* **10**, 833-839 (2015).

31. George SH, *et al.* Developmental and adult phenotyping directly from mutant embryonic stem cells. *Proc Natl Acad Sci U S A* **104**, 4455-4460 (2007).

32. Artus J, Hadjantonakis AK. Generation of chimeras by aggregation of embryonic stem cells with diploid or tetraploid mouse embryos. *Methods Mol Biol* **693**, 37-56 (2011).

33. Livak KJ, Schmittgen TD. Analysis of relative gene expression data using real-time quantitative PCR and the 2(-Delta Delta C(T)) Method. *Methods* **25**, 402-408 (2001).

34. Wingett S, *et al.* HiCUP: pipeline for mapping and processing Hi-C data. *F1000Res* **4**, 1310 (2015).

35. Langmead B, Salzberg SL. Fast gapped-read alignment with Bowtie 2. *Nat Methods* **9**, 357-359 (2012).

36. Durand NC, *et al.* Juicer Provides a One-Click System for Analyzing Loop-Resolution Hi-C Experiments. *Cell Syst* **3**, 95-98 (2016).

37. Rao SS, *et al.* A 3D map of the human genome at kilobase resolution reveals principles of chromatin looping. *Cell* **159**, 1665-1680 (2014).

38. Dobin A, *et al.* STAR: ultrafast universal RNA-seq aligner. *Bioinformatics* **29**, 15-21 (2013).

39. Lupianez DG, *et al.* Disruptions of topological chromatin domains cause pathogenic rewiring of gene-enhancer interactions. *Cell* **161**, 1012-1025 (2015).

40. Love MI, Huber W, Anders S. Moderated estimation of fold change and dispersion for RNA-seq data with DESeq2. *Genome Biol* **15**, 550 (2014).

41. Ibrahim DM, *et al.* Distinct global shifts in genomic binding profiles of limb malformation-associated HOXD13 mutations. *Genome Res* **23**, 2091-2102 (2013).

42. Lee TI, Johnstone SE, Young RA. Chromatin immunoprecipitation and microarray-based analysis of protein location. *Nat Protoc* **1**, 729-748 (2006).

43. Andrey G, *et al.* Characterization of hundreds of regulatory landscapes in developing limbs reveals two regimes of chromatin folding. *Genome Res* **27**, 223-233 (2017).

44. Ramirez F, *et al.* deepTools2: a next generation web server for deep-sequencing data analysis. *Nucleic Acids Res* **44**, W160-165 (2016).

Acknowledgments

This work was supported by a grant from the Deutsche Forschungsgemeinschaft (DFG) (MU 880/16-1) to S.M. and a UCL Award 156782/ Project 580721 to L.A. We are grateful to all members of the MPIMG transgene and mouse facility for embryonic stem cell aggregation and mouse husbandry and to all members of the MPIMG sequencing core facility.

Author Contributions

L.A. conceived the project. S.M. financed the project. A.R.R. and L.A. generated all the transgenic mouse models. L.W. performed morula aggregation. L.A. performed RNA-seq, qRT-PCRs, skeletal preparations, and phenotype analyses. A.M. performed ChIP-seq and ATAC-seq with the computational analyses performed by L.A. and A.R.R. L.A. performed cHi-C and R.S. performed the computational analysis. M.K., A.C.S., and U.F. provided technical support. A.R.R., A.M., N.B., and L.A. wrote the manuscript with input from R.S. and S.M., and approved by every co-author.

Competing interests

The authors declare no competing financial interests.

Materials and Methods

Generation of CRISPR/Cas9 genetic deletions and inversion. Genome editing experiments were performed as previously described[30]. sgRNAs were designed within close proximity of the deletion or inversion breakpoints, using the https://www.benchling.com/ platform to obtain candidate sgRNA sequences. To minimize off target effects, guide sequences were chosen to have a quality score above 95%. Complementary strands were annealed, phosphorylated, and cloned into the BbsI site of pX459 CRISPR/Cas vector (Addgene). The sequences of all sgRNAs used in this study are listed in Supplementary Table 1. G4 embryonic stem cells[31] (ESCs) (400,000) (129/Sv X C57BL/6 F1 hybrid) were seeded on CD1 mouse embryonic fibroblast (MEF) feeders and cultured under standard ESC culture conditions. The cells were transfected with 8 µg of each pX459-sgRNA construct using FUGENE HD reagent (Promega) under manufacturer conditions. After 12 hours (h), cells were split, transferred into DR4 puromycin-resistant feeders, and selected with puromycin at a final concentration of 2 µg/ml for 48 h. Clones were then grown for 5 to 6 more days, picked, and transferred onto 96-well plates on CD1 feeders. After 48h of culture, plates were split in triplicates, two for freezing and one for growth and DNA harvesting. All clones were genotyped by PCR and quantitative PCR (qPCR) analyses. Positive clones were thawed and grown on CD1 feeders until they reached an average of four million cells. Three vials were frozen, and DNA was harvested from the rest of the cells to confirm the genotyping results.

ESCs and feeder cells were tested for *Mycoplasma* contamination using the MycoAlert detection kit (Lonza) and MycoAlert Assay Control Set (Lonza). DR4 and CD1 feeder cell lines were directly produced from mouse embryos originating from DR4 and CD1 mice mattings, respectively.

Genotyping by polymerase chain reaction (PCR) and sequencing. Primers were designed at a distance of 400–500 bp from each cutting site, on both sides of sgRNA targets. Each allele has thus a set of four primers: F1(fwd)/R1(rev) amplifying one targeted site and F2(fwd)/R2(rev) amplifying the other targeted site. Deletions, duplications, and inversions were detected using the following set of primers: F1/R2, F2/R1, and F1/F2 and R1/R2, respectively. We genotyped each clone by running the PCR products on agarose gels and comparing PCR amplicon sizes. Clones showing evidence for the presence of the desired genomic rearrangement were further genotyped by Sanger sequencing. The sequences of all genotyping primers used in this study are listed in Supplementary Table 1.

Genotyping by quantitative PCR (qPCR). qPCR was performed on genomic DNA, using the QuantStudio 7 Flex Real-Time PCR System (v1.7.1) (Applied Biosystems). For the genotyping of copy number variations (CNVs), we designed four sets of primers. qPCR was carried out in a total volume of 20 µl containing 10 µl of Power Sybr Green Master Mix (Applied Biosystems), 0.4 µM of each primer and 10 ng of genomic DNA. Thermal cycling conditions were 95°C for 20 seconds (sec), followed by 40 cycles with 95°C for 3 sec and 60°C for 30 sec. A non-coding region was selected as the control amplicon. Validation experiments demonstrated that amplification efficiency of the control and all target amplicons were approximately equal. All samples were run in triplicate. The dosage of each amplicon relative to the control amplicon and normalized to wild type DNA was determined using the $2^{-\Delta\Delta CT}$ method.

Transgenic mouse strains. Mice were generated from the corresponding ESC clone by diploid or tetraploid aggregation[32], after thawing a frozen ESC vial seeded on CD1 feeders and grown for 2 days. Female mice of the CD1 strain were used as foster mothers.

All animal procedures were conducted as approved by the local authorities (LAGeSo Berlin) under the license numbers G0243/18 and G0176/19. Routine bedding, food, and water changes were performed. Mice were housed in a centrally controlled environment with a 12-h light/12-h dark cycle, temperature of 20–22.2 °C, and humidity of 30–50%. All animal experiments followed all relevant guidelines and regulations.

RNA isolation and quantitative reverse transcription PCR (qRT–PCR). To quantify RNA levels in wild type and mutant mice at E9.5, E10.5, and E11.5 developmental stages (G4 background), limb buds were micro-dissected in cold PBS, immediately snap-frozen, and stored at −80 °C. Total RNAs were extracted using the RNeasy Mini Kit (QIAGEN) according to the manufacturer's instructions. RNAs were treated with DNase I (Thermo Fisher Scientific) at 37 °C for 15 min followed by 10 min incubation at 70 °C for DNase I inactivation. Complementary DNAs (cDNAs) were generated using the Superscript III First-Strand Synthesis System (Thermo Fisher Scientific) whereby 1 µg of RNA was reverse-transcribed using oligo(dT)20. To quantify the relative abundance of transcripts, qRT–PCR analyses of 4–6 pairs of limb buds were done in technical triplicates using the Power Sybr Green Master Mix (Applied Biosystems) as described above. The dosage of each amplicon was normalized to the endogenous control amplicon (*Rps9* cDNAs). The $2^{-\Delta\Delta CT}$ method[33] was used to calculate the fold change between wild type and mutant samples. Using a one-tailed Student's *t*-test, we tested the ability of mutations to result in changes in *Gapdh*, *Maenli* and/or *En1* gene expression. The variance in mutant and wild type samples was assumed equal. The sequences of all qRT-PCR primers used in this study are listed in Supplementary Table 1.

Skeletal preparation. E18.5 fetuses (G4 background) were kept in H_2O for 1–2 h at RT and heat-shocked at 65 °C for 1 min. The skin was taken off and the abdominal and thoracic viscera were

removed using forceps. The fetuses were then fixed in 100% ethanol overnight. Afterwards, the cartilage was stained overnight using alcian blue staining solution (150 mg/l alcian blue 8GX in 80% ethanol and 20% acetic acid). Fetuses were then rinsed and post-fixed in 100% ethanol overnight. After 24 h, initial clearing was done by incubating the fetuses for 20 min in 1% potassium hydroxide in H2O, followed by alizarin red (50 mg/l alizarin red S in 0.2% potassium hydroxide) staining of bones overnight. Following this, rinsing and clearing was done for several days using low concentrations of potassium hydroxide. The stained embryos were dissected in 80% glycerol and limbs were imaged using a ZEISS SteREO Discovery.V12 with cold light source CL9000 microscope and Leica DFC420 digital camera.

Phenotypic evaluation. Phenotypic analyses for 7-8 weeks mutant mouse lines were carried out for at least 3 animals per analysis. Penetrance of the phenotypes was investigated by analyzing > 10 animals and considered fully penetrant if all animals were similarly affected.

SureSelect design. The capture Hi-C SureSelect library probes were designed over the genomic interval (mm9, chr1: 119,650,000–124,400,000) using the SureDesign online tool from Agilent.

Capture Hi-C (cHi-C). cHi-C libraries were prepared from E10.5 wild type limb buds (CD1 background). cHi-C experiments were performed as duplicates. Per biological replicate, 10 pairs E10.5 limb buds ($2\sim3 \times 10^6$ cells) were micro-dissected in PBS at RT. A single-cell suspension was obtained by incubating the tissue for 10 min at 37 °C in 1 ml Gibco trypsin-EDTA 0.05% (Thermo Fisher Scientific). Cells were resuspended in 5 ml 10% fetal bovine serum/PBS and fixed by adding 5 ml 4% formaldehyde (Sigma-Aldrich) at a final concentration of 2%. Cells were mixed for 10 min at RT. Fixation was quenched using 1.425 M glycine (Merck) on ice and immediately centrifuged at 2100 r.p.m. for 8 min. Supernatant was removed and the pellet resuspended in lysis buffer (final concentration of 10 mM Tris, pH 7.5, 10 mM NaCl, 5 mM $MgCl_2$, 0.1 M EDTA, and

1× cOmplete protease inhibitors (Sigma-Aldrich)) and incubated on ice for 10 min. Cells were then centrifuged at 2900 r.p.m. for 5 min at 4 °C, followed by removal of supernatant, snap-freezing, and storage at −80 °C. For the preparation of the 3C library, the pellet was resuspended in 60 µl 10× DpnII buffer (Thermo Fisher Scientific), and incubated with 15 µl 10% SDS for 1 h at 37 °C and 900 r.p.m. 150 µl 10% Triton X-100 was then added and the pellet was incubated for 1 h at 37 °C and 900 r.p.m. 600 µl of 1× DpnII buffer was added to the samples. A 10-µl aliquot was taken as undigested control and stored at −20 °C. The chromatin was digested using 40 µl 10 U/µl DpnII for 4 h at 37 °C and 900 r.p.m.; another 20 µl of DpnII enzyme was then added and samples were incubated overnight at 37 °C with rotation. After overnight incubation, samples were supplemented with 20 µl DpnII enzyme and incubated for four more hours at 37 °C with rotation. The DpnII restriction enzyme was inactivated at 65 °C for 20 min. Next, the digested chromatin was diluted and religated in 5.1 ml H_2O, 700 µl 10× ligation buffer (Thermo Fisher Scientific), and 1.67 µl 30 U/µl T4 DNA ligase (Thermo Fisher Scientific). Ligation reactions were incubated at 16 °C overnight with rotation. A 100-µl aliquot was taken to test ligation efficiency and stored at −20 °C. The chimeric chromatin products and test aliquots were de-cross-linked overnight by adding 30 µl and 5 µl 20 mg/ml proteinase K, respectively, and incubated at 65 °C overnight. Following this, 30 µl or 5 µl 10 mg/ml RNase A was added to the samples and aliquots, respectively, and incubated for 45 min at 37 °C. Chromatin was then precipitated by adding 1 volume phenol-chloroform to the samples and aliquots, vigorously shaking them, followed by centrifugation at 3,750 r.p.m. at RT for 15 min. The upper phase containing the chromatin was transferred to a new tube and the volume was adjusted to 7 ml with H_2O. Samples were then supplemented with 1 ml 3M NaAc, pH 5.6, 35 ml 100% ethanol, and 7 µl 20 mg/ml glycogen and frozen overnight at −80 °C. The precipitated chromatin was isolated by centrifugation at 8,350 g for 20 min at 4 °C. The chromatin pellet was washed with 10 ml 70% ethanol and further

centrifuged at 3,300 g for 15 min at 4 °C. Finally, the 3C library chromatin pellet was dried at RT and resuspended in 150 µl 10 mM Tris-HCl, pH 7.5 at 37 °C. To check the 3C library, the undigested, digested, and ligated aliquots were loaded on a 1% agarose gel. The 3C library was then sheared using a Covaris sonicator (duty cycle: 10%; intensity: 5; cycles per burst: 200; time: 6 cycles of 60 s each; set mode: frequency sweeping; temperature: 4-7 °C). Adaptors were added to the sheared DNA and amplified according to the manufacturer's instructions for Illumina sequencing (Agilent). The library was hybridized to the custom-designed SureSelect beads and indexed for sequencing (150 bp paired-end) following the manufacturer's instructions (Agilent).

cHi-C processing. FASTQ files were processed with the HiCUP pipeline v0.6.1[34] (no size selection, Nofill: 1, Format: Sanger) using Bowtie2 v2.3.4.1[35] for mapping short reads to the reference genome mm9. After the mapping, filtering and deduplication steps of the HiCUP pipeline, replicates were merged by combining their bam files. Juicer tools v1.7.6[36] was used to generate binned contact maps and to normalize maps by Knights and Ruiz (KR) matrix balancing[37]. For the generation of the contact maps, only the genomic region (chr1:120,200,001-124,400,000, mm9), part of the region enriched in the capturing step, was considered. Therefore, only read-pairs mapping to the region of interest were kept and their coordinates were shifted towards the origin by the offset of this region. Afterwards, cHi-C maps were generated with the Juicer tools 'pre' command using a custom chrom.sizes file containing only the length of the genomic region of interest (4.2 Mb) and applying a minimum MAPQ of 30. After exporting KR normalized cHi-C maps at 10kb bin size, coordinates were shifted back to mm9 coordinates. cHi-C maps were displayed as heatmaps in which values above the 98.5th percentile were truncated to improve visualization.

Virtual 4C profile generation. In order to obtain more fine-grained interaction profile for the *En1* promoter, a virtual 4C-like profile was generated from mapped, filtered and deduplicated cHi-C read pairs obtained from the HiCUP pipeline. A read-pair was considered in the profile, when it had a MAPQ≥30 and one read mapped to the defined viewpoint region while the other one mapped outside of it. Out of these pairs, reads mapping outside of the viewpoint region were counted per restriction fragment and binned to a 1kb grid. The count value of restriction fragments spanning more than one bin was distributed proportionally to the corresponding bins. Afterwards, the profile was smoothed by averaging over five bins and scaled by the factor 10^3 / counts within the enriched region. For the computation of the scaling factor, the viewpoint region and a margin ±5 kb around it were excluded. The processing was performed with custom Java code using htsjdk v.2.12.0 (https://samtools.github.io/htsjdk/).

RNA-sequencing (RNA-seq). E9.5 forelimb buds, and E10.5 and E11.5 limb buds were micro-dissected from wild type and mutant embryos (G4 background) in cold PBS, immediately snap-frozen, and stored at -80 °C. RNA-seq experiments were performed in duplicates. Total RNAs were extracted using the RNeasy Mini Kit (QIAGEN) according to the manufacturer's instructions. RNAs were treated with DNase I (Thermo Fisher Scientific) at 37 °C for 15 min followed by 10 min incubation at 70 °C for DNase I inactivation. Samples were poly-A enriched and sequenced (150 pb paired-end) using Illumina technology following standard protocols.

RNA-seq data processing. Paired-end RNA-seq reads were mapped to a custom mouse reference genome (mm9), including *Maenli* coordinates (chr1:122,744,478-122,755,676) using the STAR mapper[38] (version 2.6.1d) (splice junctions based on RefSeq; options: --alignIntronMin 20 –alignIntronMax 500000 – outFilterMultimapNmax 5 – outFilterMismatchNmax 10 –

outFilterMismatchNoverLmax 0.1). Reads per gene were counted as previously described[39], and used for differential expression analysis with the DEseq2 package[40].

ChIP-sequencing (ChIP-seq). Chromatin Immunoprecipitation was performed as previously described[41]. ChIP-seq experiments were performed in duplicates. Briefly, 10-15 pairs E10.5 or E11.5 forelimbs/hindlimbs and midbrain/hindbrain boundaries (G4 background) were microdissected in PBS at RT. A single-cell suspension was obtained by incubating the tissue for 10 min at 37 °C in 1 ml Gibco trypsin-EDTA 0.05% (Thermo Fisher Scientific). Cells were resuspended in 15 ml 10% fetal bovine serum/PBS and fixed by adding 5 ml 4% formaldehyde (Sigma-Aldrich) at a final concentration of 1%. Cells were mixed for 10 min at 4 °C. Fixation was quenched using 1.425 M glycine (Merck) on ice and immediately centrifuged at 2100 r.p.m. for 8 min. Supernatant was removed and the pellet was immediately snap-frozen and stored at -80 °C. The extraction of nuclear lysate was performed as described in Lee *et al.*[42] and chromatin was sonicated with a Diagenode Bioruptor (45 cycles with 30 sec pulse, 30 sec pause, HI power). For ChIP, 25–35 µg of chromatin was incubated with 6–8 µg of antibody (anti-H3K4me3, Millipore, cat. No. 07-473) overnight. Following this, blocked magnetic beads were added to the chromatin/ antibody mixture and incubated overnight. Next, samples were washed 6 times with RIPA buffer and one time with TE buffer[42]. After elution, the preparation of the library for pulled down DNA was performed as previously described[41]. ChIP-seq libraries were sequenced (75 bp single-end) using Illumina technology following standard protocols.

Previously published data used in this study include ChIP-seq for H3K4me3 from E10.5 forelimbs[43] and H3K4me3 from E10.5 Midbrains[16].

Transposase-accessible chromatin sequencing (ATAC-seq). ATAC-seq experiments were performed in duplicates as previously described[16]. Tissues from E11.5 embryos (G4 Background)

were microdissected in PBS at RT. A single-cell suspension was obtained by incubating the tissue for 10 min at 37 °C in 1 ml Gibco trypsin-EDTA 0.05% (Thermo Fisher Scientific). The cells were resuspended in 10% fetal bovine serum/PBS and homogenized using a 0.40 µm cell strainer (Falcon). Following this, the cells were washed in cold D-PBS (Gibco™) and lysed in fresh lysis buffer (10mM TrisHCl pH7.4, 10mM NaCl, 3mM MgCl2, 0.1% (v/v) Igepal CA-630) for 10 min while being centrifuged. Supernatant was then discarded and cells were prepared for the transposition reaction using the Nextera Tn5 Transposase (Nextera kit, Illumina). After 30 min incubation at 37° C, the nuclei solution was purified using the MinElute PCR Purification kit (Qiagen). The transposed DNA was eluted in 10µl of Elution buffer and stored at -20° C, if not immediately used. Barcoded adapters were added to the transposed DNA fragments by PCR using the NEBNext® High Fidelity 2x PCR Master Mix (NEB). To avoid saturation in our PCR reaction, we initially performed 5 cycles. Then, an aliquot of 5 µl was used to perform a qPCR in order to determine the additional number of PCR cycles needed to reach the correct amount of DNA without over-amplification. Nextera qPCR primers were used for the amplification and determination of the additional number of PCR cycles. A second round of PCR amplification using the remaining 45 µl of the 1st PCR reaction was then performed (total PCR cycles ≤ 12). Finally, the samples were purified using the AMPure XP beads (Agencourt) and eluted in 20 µl. Samples concentration was measured using Qbit and the quality was assessed using the Bioanalyzer 2100 (Agilent). ATAC-seq libraries were sequenced (75 bp paired-end) using Illumina technology following standard protocols.

ChIP-seq and ATAC-seq data processing. Single-end ChIP-seq reads were mapped with bowtie (v2.2.6)[35] to mm9, filtered for mapping quality MAPQ ≥ 10, and duplicates were removed using samtools rmdup (v1.8). For generating coverage tracks, reads were extended to 300 bp and scaled to r.p.m. (10^6 per number of unique reads) using bedtools genomecov v2.27.1.

Paired-end ATAC-seq reads were trimmed to 30 bp to allow fragments with close-by transposition events (<50 bp) to map, this increases read coverage at nucleosome-free regions. Trimmed reads were mapped with Bowtie (v2.2.6)[35], and duplicate fragments were removed using Picard RemoveDuplicates (https://broadinstitute.github.io/picard/). Coverage tracks (bigWig) were generated with deepTools (v2.0)[44] for properly mapped read pairs (FLAG 0×2) with mapping quality ≥20.